Validation of precipitation phase estimates from CloudSat-CPR across Canada

by

Rithwik Kodamana

A thesis
presented to the University of Waterloo
in fulfillment of the
thesis requirement for the degree of
Master of Science
in
Geography

Waterloo, Ontario, Canada, 2020

Author's Declaration

I hereby declare that I am the sole author of this thesis. This is a true copy of the thesis, including any required final revisions, as accepted by my examiners.

I understand that my thesis may be made electronically available to the public.

Abstract

Snow is an important component of the global climate system with significant impacts on local weather, fresh water resources, and energy balance in high latitude cold countries. Therefore precise snowfall monitoring is essential for cold countries such as Canada. Apart from the sampling issues related to access and climate in cold regions, a further significant issue that impacts snowfall monitoring is the accurate detection of precipitation phase. The CloudSat Cloud Profiling Radar (CPR) instrument is highly useful because it provides an estimate of precipitation phase along with retrievals of solid precipitation intensity. Furthermore, the sun-synchronous orbit of CloudSat allows it to have enhanced coverage over the Canadian Arctic. In this study, we validate the precipitation phase retrievals from CloudSat using the present weather information recorded on the ground by human observers (ECCC hourly weather data) from 27 stations across Canada and Precipitation Occurrence Sensor System (POSS) radar at Eureka, both maintained by Environment and Climate Change Canada (ECCC). Probability of Detection (POD), defined as the percentage of coincident CloudSat and ground observations that agree on the precipitation phase (solid, liquid or no precipitation), is used as the metric for validation. Mean POD values of CloudSat in classifying solid, liquid and non-precipitating weather at the 27 stations are 80.8%±1.5, 83.2%±1.9 and 69.8%±0.8 respectively. Binning the collocated CloudSat-ECCC hourly weather observations across Canada by the snowfall rate information available from CloudSat, we find that the accuracy of CloudSat in classifying precipitation phase increases with snowfall rate with a maximum accuracy of 85% for snowfall rates >1 mm/hr. We find that the POD varies with precipitation type, and is inversely proportional to cloud cover, with the lowest POD obtained under the heaviest cloud cover. Also, using binomial and multinomial logistic regression analysis of different physical factors, it is seen that POD of CloudSat is influenced by near-surface reflectivity, near-surface temperature and altitude of the lowest cloud layer. The results from this study imply that CloudSat has high accuracy in classifying precipitation phase and can be used to improve snowfall monitoring in cold regions.

Acknowledgements

I would like to thank my advisor, Dr. Chris Fletcher, for his excellent guidance, constructive criticism and constant encouragement. I believe the friendly interactions and the collaborative working environment really helped me grow as a researcher. Thanks to Dr. Claude Duguay and Dr. Wesley Van Wychen for coming aboard on my thesis committee and giving valuable comments on my work.

I also thank my parents Sundari and Venu and my wife, Reshma, for extending their continuous and unconditional support. I also want to thank my 'CFG Core Group' Yaassiin, Fraser, Jack, Amy and Tyler; my ENVS pals Shama, Q, Manpreet and Jaydeep; my Waterloo buddies Indranil and Yamuna; my longest-running friends Vinayak and Agnes; and my 'GD Group'. Big hugs!

I would like to express my love to my dogs, Tuttu, Kannan, Bhoora and Murphy, and all the Instagram dog accounts I follow; Thanks for keeping me happy.

As a wise man once said, "It could be better. Also, it could be worse". Thanks, CFG!

Finally, thank God.

Table of Contents

List of Tables

List of Figures

Chapter 1

Introduction

1.1 Background

Snowfall and snow cover play an essential role in the global hydrologic cycle and climate system (Field and Heymsfield, 2015). Recent studies have shown that the Arctic region is warming at a rate of two to three times faster than the global mean through Arctic Amplification, intensifying the hydrological cycle (Bintanja, 2018). The accelerated changes to winter snowfall under this changing climate can impact the flora and fauna, spring freshet, surface temperature, atmospheric dynamics, circulation patterns and permafrost extent (Norin et al., 2015; Young et al., 2018). The changes in snowfall are particularly significant for high latitude cold countries due to its influence on local weather, climate, freshwater sources, tourism, transportation and business (Kushner et al., 2018; Mudryk et al., 2018). This makes accurate snowfall monitoring essential for cold countries such as Canada.

Precipitation phase, solid or liquid, is a critical parameter that affects the accuracy of snowfall monitoring. The phase of precipitation received on the ground affects its storage (either as rain or snow), snow accumulation, water balance on glaciers and spring runoff. Past studies have shown that model predictions are sensitive to the classification of precipitation phase. Wen et al. (2013) found underestimation in simulated snow depths (SD) using Community Land Model (CLM) and coupled CLM-WRF (Weather Research and Forecasting) models due to misclassification of precipitation phase. Behrangi et al. (2018) reported up to 40% increase in simulated values of Snow Water Equivalent (SWE) related to phase misclassification. The propagation of these biases will further lead to significant errors in the estimates of streamflow, surface albedo and surface-atmosphere

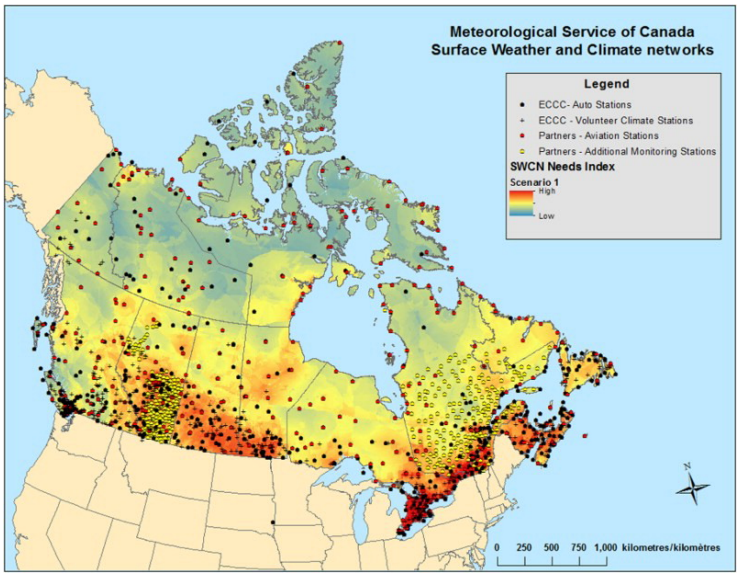

Figure 1.1: The figure shows distribution of surface weather stations across Canada. There is a sharp reduction in the density of ground-based weather stations as we go towards the Arctic (Mekis et al., 2018).

energy exchange (Jennings et al., 2018). Thus the accurate observation and recording of precipitation phase are of utmost importance.

In-situ (ground) and satellite-based instruments are widely used for observing phase information. The in-situ weather stations either accommodate a certified human observer or automated weather radars/ sensors for collecting weather (precipitation phase, intensity and prevailing weather conditions) information. However, their distribution is non-homogenous and sparse, especially over high-latitude locations, as shown in Fig. 1.1 (Behrangi et al., 2014; Norin et al., 2015; Wang et al., 2017). The coverage of ground-based weather radars is generally lacking over the polar regions, where snowfall is frequent (Norin et al., 2015). Additionally, the human-observed weather information is limited during the period of polar darkness (Lesins et al., 2010).

Space-based remote sensing is a suitable alternative to in-situ, and it provides precipitation observations on a global or quasi-global scale at a different temporal resolution than in-situ (Norin et al., 2015; Cao et al., 2014). These observations can be taken either using optical imaging satellites or by microwave remote sensing satellites. While optical imaging sensors have limited applicability in the presence of cloud-cover and require daylight for its operation (Kongoli et al., 2012), microwave remote sensing can penetrate clouds to obtain

information and works well at night (Liu et al., 2017).

Microwave remote sensing data can be retrieved either actively or passively. Passive microwave sensors measure the naturally emitted microwave radiation by the Earth's surface (König et al., 2001). In contrast, active sensors provide their own source of energy to illuminate the objects and collect observation (Zhu et al., 2017). Passive microwave instruments are widely used in the estimation of SD and SWE (Dietz et al., 2012). However, passive microwave retrievals tend to underestimate low intensity precipitation at higher latitudes, where snowfall is frequent (Behrangi et al., 2012). Additionally, the coarse spatial resolution of passive microwave sensors limits its application to monitoring snow, which are highly variable in nature (Shi, 2008).

Relative to passive, active microwave instruments come with higher spatial resolutions. Additionally, the active sensors have a distinct advantage of providing a vertical structure of clouds and precipitation (Stephens et al., 2012). Active space-based remote sensing of snowfall on a near-global scale was first made possible by CloudSat. The satellite provides snowfall observations in many high latitude remote locations between 82^oN-82^oS (Hiley et al., 2010), and it is considered as the most reliable space-based instrument available for snowfall detection (You et al., 2017). This thesis investigates the accuracy of CloudSat in identifying precipitation phases to examine its usability in improving high latitude snowfall estimates.

1.2 Methods for Identifying Precipitation Phase

1.2.1 ECCC Hourly Weather Data

The earliest continuous weather record in Canada is available for Quebec and the Hudson's Bay from the 1750s (Slonosky, 2014). Currently, the manual observing network of the Meteorological Service of Canada contains about 600 weather stations that work in participation with volunteers, aviation and other partners across Canada (Mekis et al., 2018). The stations are marked either as automated or staffed. The automated stations contain automated weather observing systems without a certified weather observer (Meteorological Service of Canada, 2015). The staffed stations house a certified weather observer responsible for recording meteorological observations. The human component involved in this measurement helps to distinguish weather types, some of which are not identified by automated instruments (Sheppard and Joe, 2000).

The human observers present at staffed weather stations classify and report present weather in every hour. Present weather is the weather conditions present at the time

of observervation (ECCC, 2011). The weather conditions include types of precipitation, weather types that obstruct vision (such as blowing snow) and sky conditions. Along with the types of precipitation, the weather records provide qualitative classification regarding precipitation intensity (light, moderate and heavy). Based on the amount of cloud cover present (in percentage), the sky conditions are marked as clear (0%), mainly clear (10-40%), mostly cloudy (40-90%) and cloudy (100%). The observations are recorded at the end of the measurement interval by a certified weather observer (Sheppard and Joe, 2008). The collected weather information is used to prepare reports with international weather codes agreed upon by the member states of the World Meteorological Organization (WMO) (Meteorological Service of Canada, 2015).

Sheppard and Joe (2000) used the human observed present weather information for validating the weather information recorded by automated sensors, which are at different temporal resolutions with moderate success. Chen et al. (2016) suggested that a validation accuracy of 69% is considered as quite good while validating CloudSat using other datasets with different spatial and temporal resolutions. The result is useful as this helps to extend the validation of CloudSat using ground-based present weather estimates, which are at different resolutions than CloudSat. Following this, this study uses the hourly human observed present weather records from 27 weather stations provided by ECCC. It is the primary source of data used for validating CloudSat precipitation phase estimates. The record includes but are not limited to the climate ID of the weather station, lat-long information, time of observation in local standard time, present weather condition, and atmospheric conditions such as humidity, temperature and dew point. The difference in temporal resolution, as well as the detection capabilities between CloudSat and human observation, brings uncertainty to the analysis. The spatial coverage of the satellite, which will not always fly above the weather station, brings additional uncertainty. The method of handling these uncertainties are described in the methodology part in Chapter 2.

1.2.2 POSS Weather Data

To collect the present weather observations at a high temporal frequency, the Meteorological Service of Canada developed the precipitation occurrence sensor system (POSS). It is a small X-band Doppler radar used for recording the occurrence, phase and intensity of precipitation (present weather information) in automated weather observing stations in every minute (Sheppard and Joe, 2008). It is a bistatic system with the transmitter and receiver mounted separately on a metallic frame 45 cm apart, as shown in Fig. 1.2 (Castellani et al., 2015). The transmitter and receiver are inclined at 20 degrees from the vertical with flat radomes for protection from the environment. Radomes or radiation domes are

the devices used to protect microwave instruments from precipitation (Rosato and Rosato, 2003). The axes of transmitter and receiver antennas intersect at the height of 34 cm above the horizontal plane passing through center points of radome (Sheppard and Joe, 1994).

Figure 1.2: The figure shows a representative POSS instrument set up at Egbert station-Ontario. It is a bistatic system with a separate signal transmitter and receiver mounted at an angle from the vertical (Sheppard and Joe, 2008).

The instrument emits horizontally polarized, low power electromagnetic waves in a continuous fashion (Sheppard and Joe, 2008, 1994). The continuous emission of electromagnetic waves by the POSS instrument does not allow it to measure time delay like other radar instruments. Instead, the sensor employs the concept of a doppler shift for measuring the Doppler velocity spectrum of falling hydrometeors. The measurement is carried out over a small sampling volume above the instrument. The sampling volume of POSS is a function of the size of hydrometeor with a maximum sampling volume of one cubic metre (Castellani et al., 2015). The Doppler signal received at the sensor is used to generate a Doppler power density spectrum. The generated power density spectrum is used to estimate the present weather information in every 1 minute (Sheppard and Joe, 2000). The minimum detection limit of solid and liquid precipitation occurrences are 0.002 mmh^{-1} and 0.001 mmh^{-1} respectively. The different types of precipitation detected by the instrument are rain, snow and drizzle (Sheppard and Joe, 2008).

This study uses present weather information from POSS using the instrument set up at Eureka, NU. The ECCC supersite at Eureka has a well-maintained record of POSS observations from 2007 overlapping with the data availability from CloudSat and ECCC hourly weather data. The higher temporal frequency of POSS (1 min) in comparison with ECCC hourly weather data helps to estimate the influence of temporal sampling in CloudSat validation results. The issues introduced by the difference in temporal and spatial sampling between POSS and CloudSat are explained in the Chapter 2 methodology section.

1.2.3 CloudSat

Satellite remote sensing provides a potential advantage in collecting precipitation information at stations situated in high latitude remote locations. CloudSat is one such satellite with a sun-synchronous orbit which helps to achieve enhanced temporal coverage over high latitudes, specifically in the Arctic (Chen et al., 2007). It is an active microwave remote sensing satellite that carries a downward-looking, non-scanning 94 GHz Cloud Profiling Radar (CPR), which retrieves backscattered power from clouds (Kulie and Bennartz, 2009; Marchand et al., 2008). The cloud scanning radar is one of the important differences between CloudSat and other operating ground-looking remote sensing satellites. The satellite has a footprint size of 1.2 km (along-track) by 1.4 km (across-track), and retrieval extends to a height of 30 km from the ground surface with a total number of 125 vertical bins. CPR has a Minimum Detectability Limit (MDL) of -28 dBZe and orbital repeat cycle of 16 days (Stephens et al., 2008). Haynes et al. (2009) reported that the high sensitivity of CloudSat-CPR enables it to detect precipitation more often than other satellites in the Arctic.

CloudSat was launched by NASA in the year 2006 to study the vertical structure of clouds from space (Kulie and Bennartz, 2009; Stephens et al., 2002). The cloud vertical structure influences the ability of clouds to produce precipitation and its intensity, radiative cooling of atmosphere, warming of earth surface through emission of radiation. The unique capability of CloudSat to sense condensed cloud particles and cloud vertical structure along with precipitation provides insights on the elementary processes by which precipitation forms (Stephens et al., 2008). The ability of CloudSat to fly in formation with the satellites in Afternoon-train constellation creates a unique multi-satellite observing system for studying the atmospheric processes necessary to the hydrological cycle (Stephens et al., 2002).

CloudSat identifies the presence of precipitation and its phase using the hydrometeor detection algorithm implemented in its 2B-GEOPROF product. The algorithm takes in

the raw radar returns recorded by CPR from the ground surface up to the height of 30 km as the input. The algorithm outputs a cloud mask with discrete values 0, 10, 20, 30 and 40, with an increase in the probability of finding hydrometeors with an increase in cloud mask value (Marchand et al., 2008). Later a spatial box filter is applied to screen out the noise signals and identify the possible occurrence of precipitation (Clothiaux and Miller, 1994). Following the identification of possible occurrence of precipitation, a simple decision tree with temperature and reflectivity thresholds are used to classify the precipitation phase and its probability. Using the temperature information available in the CloudSat ECMWF-AUX product, the maximum tropospheric temperature is estimated. The precipitation phase is set as snow when the temperature is <273 K and rain when the temperature >275 K (Smalley et al., 2014). In between these two thresholds, precipitation is identified as mixed. Later on, reflectivity thresholds are specified to estimate the probability/ certainty of finding a precipitation phase. The retrieved precipitation phases and reflectivities are further used for the estimation of snowfall and rainfall rates. The precipitation phase and snowfall rate information are available from 2C-PRECIP-COLUMN and 2C-SNOW-PROFILE products, respectively.

However, the instrumental uncertainty related to CPR and assumptions used in the algorithms leads to uncertainties in the retrieved reflectivities (Wood et al., 2014). Unlike other radar satellites or weather radars, the CPR instrument is designed to retrieve cloud properties rather than precipitation. Hence the attenuation of radar reflectivity caused by water vapour can be significant. A loss in reflectivity of up to 5 dBZe is common in the tropics (Wood, 2011). In addition to water vapour, liquid hydrometeors also attenuate radar reflectivity. The reported loss can be as high as 10 dBZe with higher liquid water contents (Wood, 2011). Similarly, high-intensity snowfall rates (between 5-16 mm hr^{-1}) can attenuate radar signals with a reported signal loss between 2 to 5 dBZe (Matrosov and Battaglia, 2009).

Additional uncertainties are introduced by the microphysical parameters and assumptions on particle shape and size distributions used to construct the scattering models. The assumed exponential distribution of particle size brings errors in reflectivity with a positive bias observed below 0 dBZe (Wood, 2011). Compact particles lead to unbiased or positively biased reflectivity estimates, while less compact particles lead to underestimation of reflectivity (Wood et al., 2014). The noise in measured reflectivity varies with signal strength and range from 3 dBZe for a reflectivity of -30 dBZe and 0.1 dBZe for reflectivities above -10 dBZe (Wood, 2011).

Surface clutter is another significant issue that contaminates the CloudSat radar returns near the ground surface (Hiley et al., 2010). Usually, the surface is a few orders of magnitude more reflective than hydrometeors. The interaction between radar pulse and

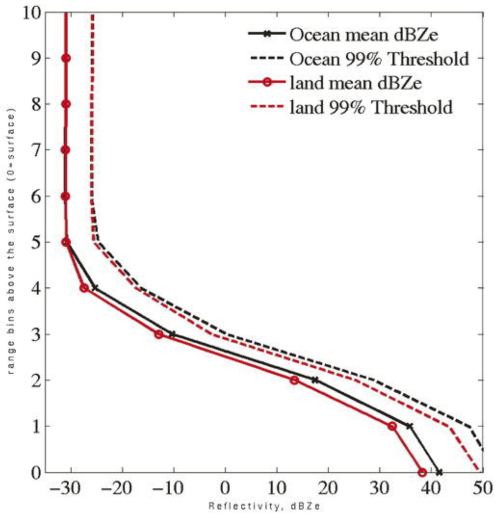

Figure 1.3: The figure shows the contamination of CloudSat radar reflectivity caused by surface clutter. There is a sharp enhancement in the reflectivity values closer to the ground surface (from 0 to 5th bin) due to interaction between surface and radar pulse (Marchand et al., 2008).

the surface causes significant enhancement of the signals, as shown in Fig 1.3. The issue impacts the bins closer to the ground surface and extends up to a height of 1.2 km (first four bins from the ground) above the surface (Marchand et al., 2008). This forces CloudSat algorithm to consider radar retrievals extracted at the forth bin above the ground (for ocean) and fifth bin above the ground (for land) as ground surface bin (Liu, 2008). Due to this, the percentage of false hydrometeor detection is twice as high between the surface and up to a height of 2 km than above 2 km (Marchand et al., 2008).

Despite these uncertainties, some of the phase validation studies of CloudSat using ground-based weather radars (Norin et al., 2015; Hudak et al., 2008) and satellite based-products (Chen et al., 2016) showed promising results. However, a validation of precipitation phase estimates from CloudSat using human-observed present weather observations (ECCC hourly weather data) over Canada has not yet been completed to my knowledge. The challenge here is to collect the sufficient number of CloudSat overpasses around the ground stations under study and to manage the temporal mismatch between CloudSat and ground-based observation. We adapt the method used by Hiley et al. (2011), for collecting overpasses that fly within a specified search radius of the ground stations. Temporal matching is carried out similar to Sheppard and Joe (2000), assuming the weather type

observed on the ground to remain as constant for a time threshold equal to the sampling frequency of ground-based datasets. Building on the previous phase validation studies, we assess the performance of CloudSat across Canada using all available matching observations from ECCC hourly weather data from 27 weather stations (2006-2016) and POSS one-minute resolution present weather data at Eureka (2007-2016).

1.3 Research Objectives

The primary objective of this thesis is to examine the usability of CloudSat in improving high latitude precipitation phase estimates. Based on the results from existing literature, we validate the precipitation phases retrieved by CloudSat using the metric Probability of Detection (POD). The validation against ground-based data will be useful in quantifying the performance of CloudSat under different precipitation/weather types and snowfall intensities.

The specific science questions to be investigated in this thesis are:

1. How well does the precipitation phase estimated by CloudSat available from its 2C-PRECIP-COLUMN product compare with ground-based ECCC and POSS present weather information?
2. Does the accuracy of precipitation phases estimated by CloudSat vary across Canada?
3. Does the performance of CloudSat's phase estimation algorithm vary under different weather types and snowfall intensity?

1.4 Thesis Structure

The objective of this chapter is to provide the necessary background information on the work described in the manuscript, which is presented in Chapter 2. The manuscript investigates the performance of precipitation phase estimates from CloudSat 2C-PRECIP-COLUMN product using ground-based present weather information. The final chapter of this thesis describes the main findings, conclusions based on Chapter 2 and potential future research.

Chapter 2

Validation of Precipitation Phase Estimates from CloudSat-CPR Across Canada

2.1 Introduction

Snow is an important component of the global climate system and cryosphere playing integral roles in Earth's water and energy balance (Derksen et al., 2012; Thackeray et al., 2015). Snow covers approximately 47 million sq. km on average of Northern Hemisphere each year (Robinson and Frei, 2000; Thackeray et al., 2014). Snowfall readily changes the surface temperature, impacts atmospheric dynamics and circulation patterns and effects permafrost extent (Birkeland and Mock, 1996; Norin et al., 2015). Snow cover is particularly important to the cultural identity and economy of Canada through its influence on short-term weather and long-term climate by altering the surface energy budget, local interactions with wind and temperature in the Arctic and other snow-covered regions, freshwater storage, tourism and transportation (Mudryk et al., 2018; Barnett et al., 2005; Flanner et al., 2011). Therefore, precise snowfall monitoring is essential for high latitude countries such as Canada.

Snow monitoring at ground-based weather stations is often carried out by trained human observers using present weather information or by using automated weather radars/ sensors. The human component involved in weather measurement helps to distinguish weather types, some of which are not identified by automated instruments (Sheppard and Joe, 2000). Across Canada, Environment and Climate Change Canada (ECCC) maintains

a network of 1735 surface weather stations, but this network is sparse in remote regions such as the Canadian Arctic, where snowfall is frequent, due to challenges related to access and climate (Mekis et al., 2018). Snow cover and snow mass are known to be highly variable in space, and so the in situ measurement network in Canada may be too sparse to obtain reliable snowfall estimates over an entire region (Kulie and Bennartz, 2009; Shi, 2008). A further significant challenge which influences the accuracy of snow monitoring is in the accurate detection of the different precipitation phases (snow or rain) in the Arctic. Different phases of precipitation affect land hydrology and climate differently (Dai, 2008). Misclassification of precipitation phase causes substantial errors in the estimates of Snow Water Equivalent (SWE), snow depth (SD), snowfall rate, snow albedo feedback and streamflow (Mizukami et al., 2013; Wen et al., 2016; Wayand et al., 2017; Jennings et al., 2018). Additionally, human observations of precipitation phase at high latitudes are made very challenging by the long periods of darkness during polar night (Intrieri and Shupe, 2004).

Satellite remote sensing provides the potential to overcome several of these challenges by providing global or quasi-global observations of frozen precipitation (Cao et al., 2014). Passive microwave sensors have been used to estimate snow properties across Canada with moderate success (Derksen and Walker, 2003; Foster et al., 2005); however, passive microwave retrievals tend to underestimate low-intensity precipitation occurrences at higher latitudes (Behrangi et al., 2012; Tang et al., 2014). Also, the coarse spatial resolution of passive microwave satellites limits its application to monitoring snowfall, which are highly variable in nature (Dietz et al., 2012; Shi, 2008). Relative to passive, active microwave sensors present the advantage of having a higher spatial resolution. Furthermore, active radar instruments such as the Cloud Profiling Radar aboard the CloudSat satellite provides information on the vertical structure of clouds and precipitation (Stephens et al., 2012). Active space-borne snowfall observations on a near-global scale were first made possible by CloudSat, providing snowfall observations in many remote, high latitude locations between 82^oN-82^oS (Liu, 2008; Hiley et al., 2010). The near-daily high latitude coverage and high radar sensitivity of CloudSat make it ideal for snowfall research in the Arctic (Kulie et al., 2016).

However, several instrumental and environmental factors impact CloudSat's ability to retrieve surface snowfall accurately. The 94 GHz radar instrument on-board CloudSat is designed to retrieve cloud properties, rather than precipitation. Therefore water vapour, liquid and frozen hydrometeors may attenuate the CloudSat radar retrieval (Wood, 2011). Surface clutter, due to radar pulses interacting with the ground surface, is another significant issue that contaminates CloudSat retrievals of precipitation phase and snowfall rates within the boundary layer (Hiley et al., 2010). Despite these challenges, some of the recent

validation studies of surface precipitation phases retrieved by CloudSat using the Canadian C-Band, NEXRAD and SWERAD radar networks and remote sensing products have shown promising results (Hudak et al., 2008; Norin et al., 2015; Cao et al., 2014; Smalley et al., 2013). However, a detailed validation of CloudSat precipitation phase estimates using ground-based present weather information over Canada has not yet been completed to our knowledge.

The primary goal of this work is to validate the precipitation phase estimates of CloudSat using ground observations and to evaluate its usability for providing improved snowfall estimates over high latitude locations where there are no ground stations. We also aim to determine whether CloudSat's accuracy varies for different weather conditions and precipitation intensities. Section 2 introduces the datasets used in this study, along with details of the data processing and validation methodology. Section 3 and 4 comprise the phase validation results of CloudSat using ground observations followed by section 5, discussing the essential findings and potential future research.

2.2 Datasets & Methodology

2.2.1 ECCC Hourly Weather Data

ECCC provides hourly observations of weather/precipitation types (will be referred to as 'ECCC weather data' for the rest of this paper) recorded by trained human observers positioned at designated weather stations. Human observers report different types of solid, liquid and non-precipitating weather types, some of which are undetectable to ground and space-based radars (Sheppard and Joe, 2000), but they may also miss particular events such as light precipitation, or virga (Merenti-Välimäki et al., 2001). The weather types included in the study are snow grains, snow showers, snow, moderate/heavy snow, freezing drizzle, drizzle, thunderstorms, rain, rain showers, moderate/heavy rain, cloudy, mostly cloudy, mainly-clear and clear. Ice crystals which are produced either by boundary layer clouds or as diamond dust from cloudless sky (Intrieri and Shupe, 2004) are excluded from the analysis because of ground clutter contamination in CloudSat retrievals (Marchand et al., 2008).

We simplified the analysis by combining the different types of solid precipitation recorded by the ECCC observer into a single group called 'solid precipitation', liquid precipitation types as 'liquid precipitation' and non-precipitating types as 'non-precipitating weather' (Dai, 2008; Jennings et al., 2018). This grouping allows for a cleaner comparison with

CloudSat, which only classifies the occurrence of snow (solid precipitation), rain (liquid precipitation) or no precipitation. The grouped solid, liquid and non-precipitating ECCC observations are used to validate the estimated precipitation phase from CloudSat retrievals.

2.2.2 POSS Weather Data

Precipitation Occurrence Sensor System (POSS) is a ground-based, upward-looking X-band radar that provides an estimate of precipitation phase and its intensity (mm/hr) at a temporal resolution of 1-minute (Sheppard, 2007; Sheppard and Joe, 2008). POSS measures the Doppler signal of falling hydrometeors through a small sampling volume, proportional to the size of hydrometeor. The maximum size of the sampling volume is limited to one cubic metre. The instrument uses the measured Doppler signal for the estimation of present weather information and precipitation intensity (Castellani et al., 2015).

Owing to the higher temporal sampling rate of POSS compared to ECCC present weather observations (1 hour), the POSS instrument provides independent verification of the influence of temporal sampling in CloudSat validation accuracy. Similar to ECCC weather data, the different solid precipitation types recorded by POSS are grouped into a single group called 'solid precipitation', liquid precipitation types as 'liquid precipitation' and non-precipitating types as 'non-precipitating weather', for validating the precipitation phase of CloudSat retrievals.

2.2.3 CloudSat

NASA launched CloudSat in the year 2006, and it carries a 94 GHz Cloud Profiling Radar (CPR) (Stephens et al., 2008). The CPR retrieves the backscattered power from cloud droplets for each retrieval made by CloudSat along its track (Chen et al., 2007; Marchand et al., 2008). The orbital track covered by CloudSat is its overpass, which is made up of individual CPR retrievals. Each CPR retrieval contains radar returns recorded in every 0.16 seconds from the ground surface up to a height of 30km split into 125 vertical bins, each of 240m in height. Table 2.1 shows the CloudSat data products used in this study. 2B-GEOPROF is the preliminary product that identifies the occurrence of precipitation at the surface using the raw radar returns recorded by CPR for each retrieval (Marchand et al., 2008). CloudSat algorithm uses the ECMWF-AUX dataset for classifying the phase of precipitation. It is an observation based operational analysis product that provides

Table 2.1: Variables extracted from CloudSat

CloudSat Product	Extracted Variables	Units
ECMWF-AUX	2m temperature	K
2C-PRECIP-COLUMN	Precipitation flag	-
	Melted mass fraction	-
	Near surface reflectivity	dBZe
	Cloud top height	km
2C-SNOW-PROFILE	Surface snowfall rate	mm/hr

the set of ancillary ECMWF state variables interpolated to CPR radar bins (Cronk and Partain, 2017; ECMWF, 2019).

The phase of precipitation received at the surface for each CloudSat retrieval is marked as snow (Temperature, T<0 ^{o}C from ECMWF-AUX), mixed (0<T<2 ^{o}C) or rain (T>2 ^{o}C) (Smalley et al., 2014). The estimated phase of precipitation is available from the 2C-PRECIP-COLUMN product as precipitation flags (Smalley et al., 2014). Later on, for the retrievals identified as snow in 2C-PRECIP-COLUMN, using the reflectivity values for the ground surface bin, the assumed particle size distribution, and microphysical parameters, the cloudsat snowfall estimation algorithm is run to estimate the snowfall rate at the surface. The snowfall rate at the surface is available from the 2C-SNOW-PROFILE product.

The uncertainty in retrieved CloudSat reflectivity due to topography appears as ground clutter (Palerme et al., 2017), which enhances the radar reflectivity values close to the ground surface. The contamination of radar signals caused by ground clutter is avoided in the retrievals by considering the fourth bin above the ground (for ocean) or the fifth bin above the ground (for land) as ground surface bin (Liu, 2008). The uncertainty in precipitation retrievals over different surface types are reduced by using an improved method in determining path integrated attenuation (Haynes and L'Ecuyer, 2013). In this study, CloudSat overpasses that fall within a 100 km spatial radius centred on each ECCC ground station under consideration are collected (Fig. 2.3(a)). The precipitation flag, which estimates the precipitation phase (solid or liquid) received at the surface for each retrieval is aggregated to estimate the precipitation phase of each overpass. The proportion of solid and liquid precipitation flags in an overpass are compared to classify the precipitation

phase of that overpass.

$$Solid\ Proportion,\ SP = \frac{N_{sf}}{N} \tag{2.1}$$

$$Liquid\ Proportion,\ LP = \frac{N_{lf}}{N} \tag{2.2}$$

where N_{sf} = number of retrievals flagged as solid in an overpass; N_{lf} = number of retrievals flagged as liquid in an overpass; N = total number of retrievals in an overpass.

An overpass is identified as 'solid precipitation' when SP>LP or else it is classified as a 'liquid precipitation'. An overpass is non-precipitating when SP=LP=0. The snowfall rate for each overpass is computed as the mean of the surface snowfall rate of individual retrievals contained in that overpass. The occurrences of mixed precipitation (identified with 'mixed precipitation flag') are converted into solid or liquid based on the value of the melted mass fraction. Melted mass fraction is the mass fraction of snow that has undergone melting. CloudSat snow estimation algorithm considers mixed precipitation occurrences with melted mass fraction values <=0.15 as snow, and a surface snowfall rate is estimated for these cases (Stephens and Wood, 2013). The same rule is followed in this study for the conversion of mixed precipitation occurrences to solid (melted mass fraction <=0.15) or liquid (melted mass fraction >0.15).

2.2.4 Method of Validation

Our validation procedure for CloudSat precipitation phase assumes that the weather type recorded on the ground remains constant for a time threshold of τ, where τ is the sampling frequency of ground-based datasets (for ECCC τ = 1 hour and for POSS τ = 1 minute) (Sheppard and Joe, 2000; Norin et al., 2015; Chen et al., 2016). The temporal collocation of processed CloudSat overpass data with ground-based weather datasets is carried out by considering $\tau/2$ as the maximum time difference between CloudSat and ground-based datasets. The Probability of Detection (POD) metric is used to quantify how often CloudSat detects the same precipitation phase as either ECCC or POSS. It is defined as the percentage of weather events of each type wherein precipitation phase of CloudSat overpass agreed with the corresponding precipitation/weather type recorded on the ground by ECCC and POSS weather datasets. Contingency tables are defined to estimate the POD of CloudSat for solid, liquid and non-precipitating weather for ground-based datasets.

A sensitivity analysis is carried out to decide the spatial radius used for collecting CloudSat overpasses around weather stations. Analysis carried out using the collocated CloudSat-ECCC overpasses at Eureka weather station shows similar POD values for different spatial radii, as shown in Fig. 2.1. The confidence intervals represent 95% confidence intervals in POD. Afterward, a spatial radius of 100km is selected as it provides the optimum balance between sample size and distance from stations used in this research. The selected spatial radius provides an adequate number of overpasses (sample size) over the ground stations shown in Fig. 2.2 with reduced spatial uncertainty. The variation of POD across Canada is estimated by combining the data available from 27 weather stations (refer Table 2.2).

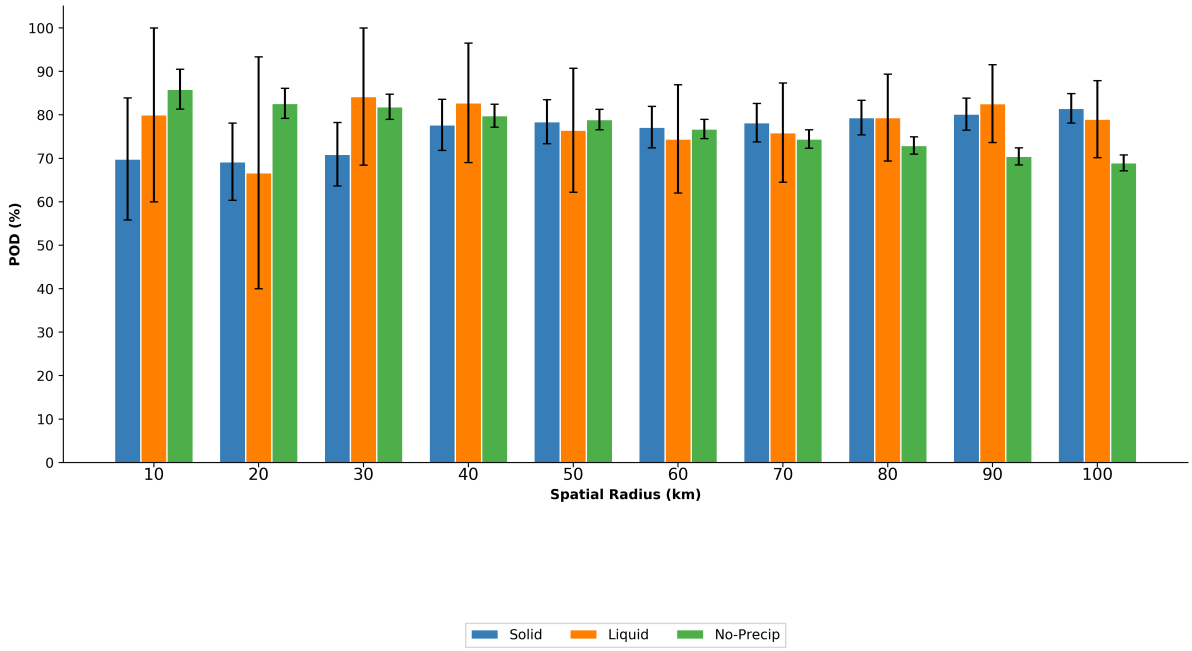

Figure 2.1: The figure shows POD of CloudSat in classifying solid, liquid and non-precipitating conditions for different spatial radii varying from 10km to 100km

The primary study site considered in this analysis is Eureka, Nunavut due to the availability of a large number of CloudSat overpasses and the overlapping data availability from CloudSat, ECCC and POSS weather datasets from July 2006 to December 2016. A detailed case study is carried out at Eureka to demonstrate the usage of precipitation flags for phase validation. Later, POD of CloudSat in identifying solid, liquid and non-precipitating weather is estimated separately using ECCC and POSS weather datasets

Table 2.2: Table showing the geographical co-ordinates of stations considered in this study, number of solid, liquid and non-precipitating CloudSat overpasses (sample size) obtained after collocating CloudSat and ECCC weather data

Sl No.	Station	Lat (^{o})	Lon (^{o})	Solid	Liquid	No-Precip
1	Eureka	79.99	-85.93	503	81	2407
2	Resolute-Bay	74.72	-94.97	388	85	725
3	Inuvik	68.67	-133.68	162	83	632
4	Norman Wells	65.28	-126.80	151	53	607
5	Iqaluit	63.75	-68.54	114	55	486
6	Mayo	63.62	-135.87	86	56	631
7	Churchill	58.73	-94.07	96	29	321
8	Kuujjuaq	58.34	-68.38	165	102	488
9	Gilllam	56.34	-94.70	86	40	415
10	La Ronge	55.11	-105.29	84	28	476
11	Kindersley	51.52	-109.18	32	37	486
12	Blanc Sablon	51.44	-57.13	56	75	425
13	Calgary	51.11	-114.02	39	28	389
14	Red Lake	51.09	-93.69	63	37	190
15	Kapuskasing	49.40	-82.41	94	61	411
16	Vancouver	49.25	-123.12	2	85	446
17	Thunder-Bay	48.45	-89.32	44	38	336
18	St. John's	47.62	-52.74	38	86	263
19	Quebec	46.83	-71.25	51	63	399
20	Sault Ste Marie	46.57	-84.41	61	52	341
21	North-Bay	46.40	-79.39	78	56	326
22	Charlottetown	46.29	-63.13	34	46	245
23	Montreal	45.47	-73.74	44	51	370
24	Ottawa	45.32	-75.67	27	44	354
25	Halifax	44.88	-63.51	35	70	342
26	Toronto	43.68	-79.63	16	38	316
27	London	43.00	-81.25	39	43	257
	TOTAL			2588	1522	13084

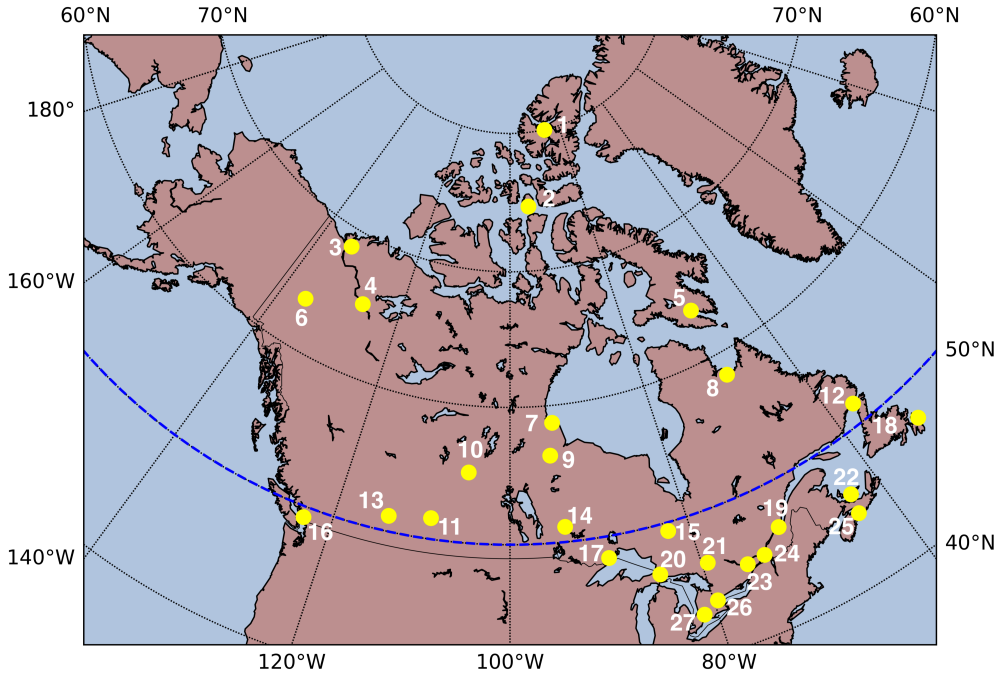

Figure 2.2: The figure shows distribution of weather stations used in this study as listed in Table 2.2. 1. Eureka, WEU; 2. Resolute-Bay, YRB; 3. Inuvik, YEV; 4. Norman Wells, YVQ; 5. Iqaluit, YFB; 6. Mayo, YMA; 7. Churchill, YYQ; 8. Kuujjuaq, YVP; 9. Gillam, YGX; 10. La Ronge, YVC; 11. Kindersley, YKY; 12. Blanc Sablon, YBX; 13. Calgary, YYC; 14. Red Lake, YRL; 15. Kapuskasing, YYU; 16. Vancouver, YVR; 17. Thunder Bay, YQT; 18. St. Johns, YYT; 19. Quebec, XBO; 20. Sault Ste Marie, YAM; 21. North Bay; YYB; 22. Charlottetown, YYG; 23. Montreal, YUL; 24. Ottawa, YOW; 25. Halifax, YHZ; 26. Toronto, YYZ; 27. London, YXU. The dotted blue line shows the distribution of stations on either side of 50°N, which will be referred to in the pan-Canada validation section.

at this station. Acknowledging the inherent differences between ground-based ECCC and POSS radar observations, a dataset (will be referred to as 'CloudSat-ECCC-POSS dataset' for the rest of this paper) is created by collocating all three datasets (CloudSat, ECCC and POSS) at Eureka. Analysis is carried out to identify the impacts of different precipitation/ weather types recorded on the ground surface and snowfall intensity in deciding the POD of CloudSat at Eureka and pan-Canada. The POD for individual weather types is estimated only if its sample size is >20. The snowfall rate from CloudSat is used to estimate the

variation of POD with precipitation intensity.

2.3 Validation at Eureka, NU

2.3.1 Snowfall Event on 18 October 2006

To illustrate how our phase classification and validation method works, Fig. 2.3(b) shows an overpass recorded within the 100 km spatial radius around the Eureka weather station on 18 October 2006 at UTC 15:33. The colour-code of the overpass follows the precipitation flags recorded by CloudSat every 0.16 seconds along its orbital path close to the weather station. Figures 2.3 (c), (d), and (e) represent the reflectivity, snowfall rate and temperature profiles for the same overpass recorded by CloudSat from the ground surface up to 14 km. The overpass captures a precipitation event as it moves from right to left. It is indicated by the colour change of overpass (precipitation flag) from green (no-precipitation) to orange (liquid) and blue (solid) in Fig. 2.3(b). The presence of precipitation is identified with the sudden increase in reflectivity in Fig. 2.3(c). The snowfall rate profile (Fig. 2.3(d)) indicates the snowfall rates measured in atmosphere corresponding to the increases in radar reflectivity and can be used to detect the presence or absence of solid precipitation. The gaps in the snowfall profile indicate the absence of solid precipitation and when combined the Fig. 2.3(b) (overpass colored with precipitation flag) helps to identify the locations of possible rain occurrences. The temperature profile (Fig. 2.3 (e)) shows temperature close to 0 ^{o}C near the ground surface throughout this overpass. This suggests that the precipitation event is occurring in a snow-rain transitional environment.

The ground clutter contamination of CPR retrieval is indicated as the absence of data from the ground surface up to 1.2 km in Figures 2.3 (c), (d) and (e). The higher reflectivity values towards the ground surface indicate that the hydrometeors grow as they fall (Fargey et al., 2014). The bright band (a region with enhanced reflectivity) is situated at the height of 3 km from the ground surface in Fig. 2.3 (c) and moves closer to the ground surface as the satellite moves north. Snowflakes covered in liquid water and signal attenuation caused by liquid hydrometeors produce bright bands (Sassen et al., 2007; Matrosov, 2014). The slight reduction in reflectivity below the bright band along with the coincident increase in temperature indicates the melting of snowflakes (Fall et al., 2013). The locations of sharp reduction in reflectivity (centred around UTC 15:34:00 and 15:34:10 in Fig. 2.3 (c)) indicate the complete conversion of snowflakes to raindrops. This phase change is marked by the change in precipitation flag from solid to liquid (colour change from green and blue to orange) in Fig. 2.3 (b) and gaps in vertical profiles of snowfall rate in Fig. 2.3 (d).

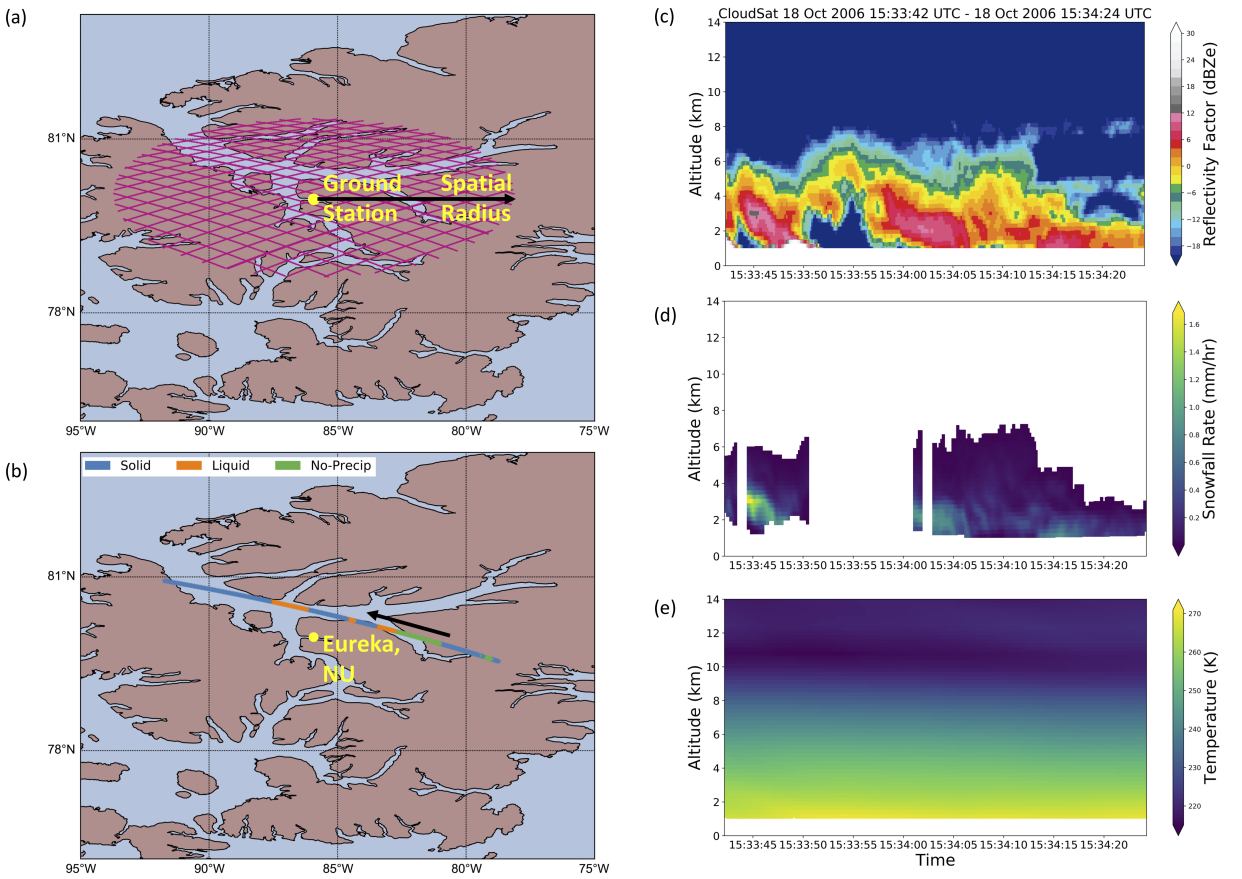

Figure 2.3: (a) A spatial radius (100 km) is specified to obtain the CloudSat overpasses around each ground station considered in this study. Purple lines represent individual overpasses, which are made up of individual retrievals recorded every 0.16 seconds. (b) shows a CloudSat overpass that relates to panels (c)-(e), recorded on 18 October 2006 at UTC 15:33 near the Eureka weather station. The overpass is colour-coded based on type of precipitation flags retrieved. The black arrow in (b) indicates the direction of travel of the satellite. (c), (d), and (e) show the CloudSat reflectivity, snowfall rate and temperature profiles for the same overpass.

The proportion of CloudSat retrievals with flags indicating solid, or liquid, for this overpass are SP = 0.64 and LP = 0.19, respectively, with the remaining 17% of retrievals showing no precipitation. Because SP>LP, this overpass is classified as a solid-precipitation

overpass. The ECCC present weather information recorded at the time (UTC 16:00) closest to the CloudSat overpass (UTC 15:33) indicates 'snow' as the precipitation type received on the ground. The precipitation phase of the overpass agrees with the weather type recorded on the ground and constitutes a successful classification (a 'hit'). As the different types of ECCC solid precipitation types are grouped and considered under a single group 'solid precipitation', the result would be considered as a 'hit' even if the ground has reported any other type of solid precipitation (for, eg. light snow, snow grains etc.). If the precipitation phase of CloudSat overpass is not in agreement with the ECCC present weather observation closest in time, then that overpass would be recorded as a 'miss'. In the same manner, for each ECCC ground station, each overpass with a matching present-weather observation within 30 minutes is classified and recorded as a hit or miss. The POD is calculated as the total number of CloudSat overpass hits divided by the total number of matching overpasses.

2.3.2 Validation for Precipitation Occurrence and Phase

Expanding this methodology to all n=2991 coincident CloudSat-ECCC overpasses at Eureka (Table 2.2), we find POD values of 81.5%, 79%, and 69% for solid, liquid and no-precipitation, respectively, as indicated by the diagonal elements of Table 2.3. The POD values show that CloudSat has high accuracy in identifying solid and liquid precipitation with a lower POD for non-precipitating conditions. The results are particularly significant if we think of the spatial and temporal mismatch between CloudSat and ECCC weather data. First of all, CloudSat records are based on overpasses, which occur at a few km away from the station (most of the cases). The POD values are based on the comparison of the precipitation phase of those overpasses with ECCC present weather observations recorded within a 30 minute time difference at the station.

We find similar POD values (78.4%, 76.5% and 71.1% for solid, liquid and non-precipitation respectively) for CloudSat against the POSS weather data as indicated by the diagonal elements in parentheses in Table 2.3. The fact that similar POD values are obtained by comparing CloudSat with two independent ground-based observing systems gives confidence in the precipitation phase estimates from CloudSat. Since CloudSat looks downward from space with up to a 30 minute offset from the ECCC (ECCC hourly data) sampling, and POSS looks upward from the surface with consistent 1-minute sampling, the results suggests that ground clutter and temporal sampling do not have a major impact on the estimates of precipitation phase from CloudSat. Additionally, the CloudSat POD values of solid precipitation obtained in this analysis are better than the POD value of 69% reported by Chen et al. (2016). The results from this analysis give further confidence in the

Table 2.3: Contingency table showing the POD calculated between CloudSat and ground-based ECCC and POSS (in parentheses) at Eureka station. The POD of CloudSat using POSS data is shown in brackets. The sample size for the POSS data is: Solid - 291; Liquid - 81; No-Precip - 3008

ECCC(POSS) / CloudSat	Solid	Liquid	No-Precip
Solid	81.5 (78.4)	6.2 (8.6)	24.9 (24.0)
Liquid	0.6 (0.7)	79.0 (76.5)	6.1 (4.9)
No-Precip	17.9 (20.9)	14.8 (14.9)	69.0 (71.1)

pan-Canada application of this phase validation methodology, which will be discussed in the coming sections. POD values of CloudSat estimated using the CloudSat-ECCC-POSS dataset are 87.1%, 82.9% and 75.4% respectively for solid, liquid and non-precipitating weather conditions (Table not shown). Even with the use of the CloudSat-ECCC-POSS dataset, CloudSat seems to miss (or misclassify) several solid, liquid and non-precipitating weather occurrences.

It is encouraging to see that CloudSat misclassified only a tiny fraction of solid precipitation recorded by ECCC and POSS weather data (<1%) as liquid precipitation (refer Table 2.3). The high accuracy for solid precipitation also has to do with the cold climatological conditions at Eureka. The annual mean temperature based on 12 years of ECCC weather data at Eureka is -18^{o}C. The classification of solid precipitation as liquid occurred only on those days when the temperature recorded on the ground was close to 2^{o}C. Theses cases hint towards the temperature threshold based separation used in the CloudSat algorithm for identifying precipitation phases.

2.3.3 Validation for Different Precipitation/Weather Types

In order to better understand the influence of weather/precipitation type on CloudSat accuracy, we estimate the POD of CloudSat under different solid, liquid and non-precipitating weather types. Fig. 2.4(a) shows the CloudSat POD values for different solid, liquid and non-precipitating weather types estimated using ECCC weather data as the reference at Eureka. Most of the solid precipitation falls in the form of snow (94.6% of total solid precipitation), and the POD for snow is 82.3%. Very few events of other solid precipitation types (snow grains (n=18) and snow showers (n=8)) occur at Eureka. These two types

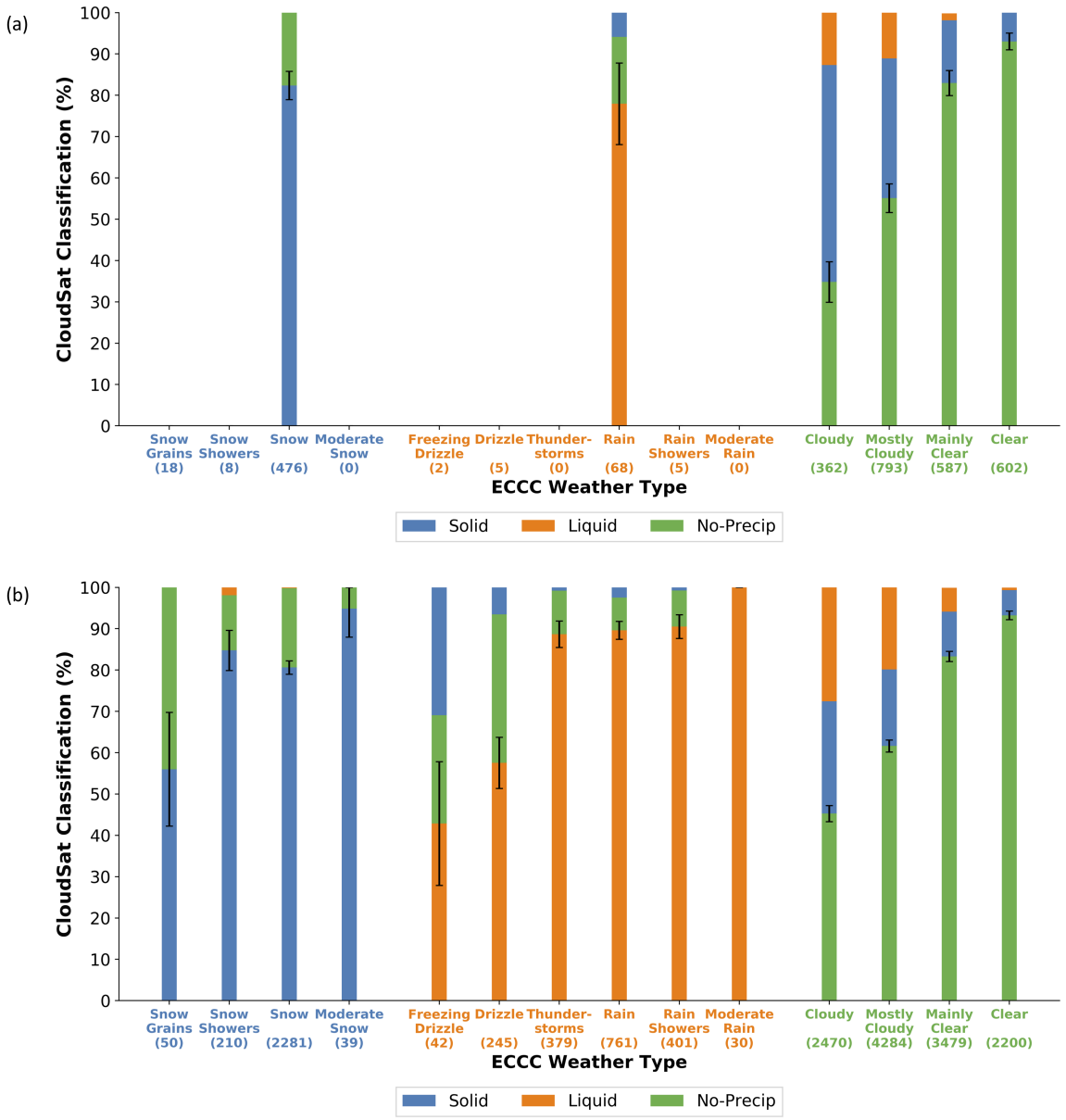

Figure 2.4: The precipitation phases classified by CloudSat against different ECCC hourly weather types recorded on the ground at Eureka (a) and pan-Canada (b). The bars closest to the x-axis represent CloudSat POD. The sample size for each type is given in parentheses.

have a combined POD of 53% (not shown in Fig. 2.4 (a)). Most of the liquid precipitation occurs as rain (84% of total liquid precipitation), and POD for rain is 77.9%. The rest of the liquid precipitation at Eureka is a mix of rain showers, drizzle and freezing drizzle, which are too small in number if considered separately. Out of these, CloudSat correctly classified all 'rain shower' (n=5) occurrences and 5 drizzle/ freezing drizzle occurrences (n=7). It is challenging to estimate the POD for precipitation types other than snow and rain due to the small number of events at Eureka. In the case of non-precipitating weather types, 'clear' and 'mainly clear' weather conditions are characterized by high POD values of 93% and 83%, respectively. The low accuracy of CloudSat in identifying 'cloudy' (34.8%) and 'mostly cloudy' (55.1%) weather types as non-precipitating reduces the overall POD of CloudSat for non-precipitating weather.

Hudak et al. (2008) suggested that the reflectivity threshold used in the CloudSat precipitation occurrence algorithm could misclassify virga clouds as precipitation occurrences. Virga precipitation is where water or ice particles falling from a cloud evaporate or sublimate before reaching the Earth's surface (Wang et al., 2018). Wang et al. (2018) suggested that CloudSat CPR due to its higher sensitivity towards low-intensity precipitation is more prone to capture virga occurrences as precipitation. This study identifies virga precipitation as the cases where the two sensitive radar sensors (CloudSat and POSS) detected precipitation, but the human observers detected no precipitation. Further analysis using CloudSat, ECCC and POSS weather data for the commonly available dates at Eureka suggests that CloudSat is misclassifying 16.4% of virga clouds as precipitation. The obtained virga percentage is close to the value found by Wang et al. (2018) using CloudSat in the Arctic.

2.4 Validation Across Canada

2.4.1 Precipitation Occurrence and Weather Type

Extending this validation to the full set of ECCC weather stations (n=27, Fig. 2.2) shows that the CloudSat POD values across Canada are broadly consistent with those reported at Eureka (Fig. 2.5), with some notable differences. Mean POD value computed for solid, liquid and non-precipitating conditions across Canada are 80.8%±1.5, 83.2%±1.9 and 69.8%±0.8 respectively (Table 2.4). The uncertainty ranges represent the 95% confidence intervals in POD. Similar to Eureka, high accuracy values are noted for snow and rain and low accuracies for cloudy and mostly cloudy weather conditions. Also, low POD is noted in cases of snow grains (56%), drizzle (57.6%) and freezing drizzle (42.9%), with the satellite

Table 2.4: Contingency table showing the POD calculated between CloudSat and ECCC weather data across Canada. The sample size for the collocated dataset is: Solid - 2588; Liquid - 1522; No-Precip - 13084

CloudSat \ ECCC	Solid	Liquid	No-Precip
Solid	80.8	2.6	17.0
Liquid	3.2	83.2	13.2
No-Precip	16.0	14.2	69.8

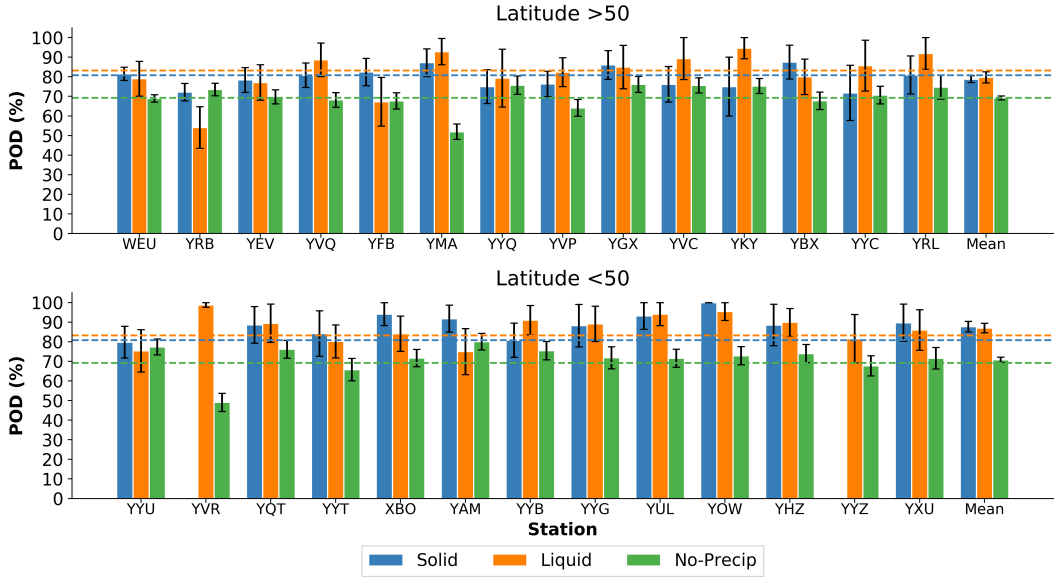

Figure 2.5: Variation of CloudSat POD across Canada. Sample size used for individual stations are given in Table 2.2.

seems to miss the occurrences of snow grains and drizzle (Fig. 2.4(b)). The impacts of drizzle and freezing precipitation types on POD are visible at Resolute-Bay station, which lowers its POD value for liquid precipitation to 54.1% (Fig. 2.5). Compared to Eureka, there is a pan-Canada increase in the percentage of solid precipitation cases misclassified as liquid and a decrease in liquid precipitation misclassified as solid. Also, outside Eureka,

several cases are observed where the non-precipitating conditions are misclassified as a liquid rather than solid. It is reasonable to assume that some/all of these differences are explained by the very different climatological and environmental conditions experienced at the pan-Canadian stations compared to those in Eureka.

The mean temperature for the misclassified cases where solid precipitation classified as a liquid is 0.4^{o}C. This is consistent with the influence of threshold temperatures (0 ^{o}C for solid and 2 ^{o}C for liquid) used in the CloudSat algorithm in classifying the precipitation phase (Smalley et al., 2014). The pan-Canada reduction in the cases where liquid precipitation is misclassified as solid compared to Eureka has to do with the increase in sample size as well as the occurrence of liquid precipitation events considerably above 0^{o}C, outside the Arctic. Additionally, the pan-Canada increase in non-precipitating weather conditions misclassified as liquid could be due to the increase in temperature and more number of water clouds encountered by the satellite at low latitude stations.

2.4.2 Influence of Precipitation Intensity

In this Section, motivated by our understanding of the sensitivity of CloudSat-CPR to precipitation intensity, we investigate to what extent POD may vary as a function of solid precipitation intensity. We begin by identifying all matched CloudSat-ECCC observations with nonzero CloudSat retrieved surface snowfall rates (SR, units mm/hr). Next, we bin this set of n=4058 cases into 8 groups by SR and recompute the POD for the cases in each group, and these results are shown in Fig. 2.6. The error bars represent 95% confidence intervals in POD. POD is estimated as the percentage of CloudSat snow occurrences classified as solid precipitation by ECCC weather data. We note that CloudSat does not a provide rain rate product over land (Lesbock, 2018), and therefore the variation of POD with rain rate is not estimated. However, we do show the frequency of cases where CloudSat classifies solid precipitation and ECCC observed liquid.

Fig. 2.6 shows that, for our pan-Canada dataset, a relatively lower accuracy is noted for intensities <0.01 mm/hr (33.9%), followed by a steady increase in accuracy with an increase in SR (85% for >1 mm/hr). Chen et al. (2016) reported a broadly similar variation of increase in CloudSat POD with intensity, with a POD $\sim$ 76% reported for SR between 1-2.5 mm/hr. CloudSat has a higher sensitivity for low-intensity snowfall. This observational advantage allows it to detect low-intensity precipitation events, which remain mostly undetectable to a human observer. Also, CloudSat due to its high sensitivity is reported to capture virga clouds as precipitation ($\sim$ 20% in latitudes above 60 ^{o}N (Wang et al., 2018)). The difference in sensitivities between the human observer and CloudSat leads to

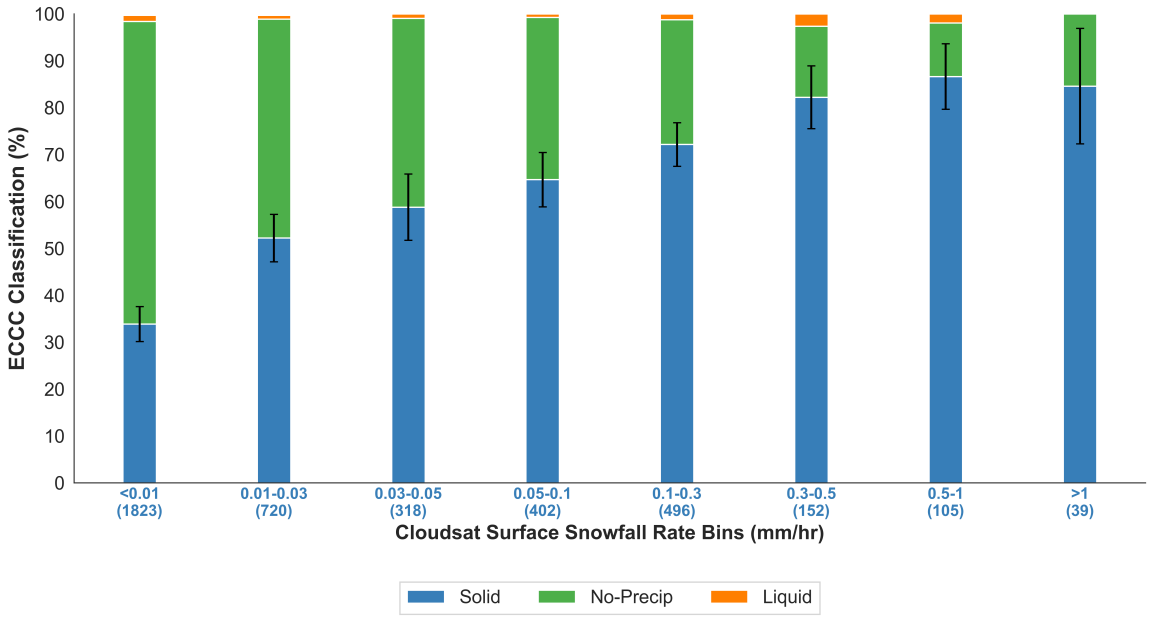

Figure 2.6: Percentage of CloudSat solid precipitation occurrences detected on the ground by the human observer (ECCC Weather data) binned using the snowfall rate information available from CloudSat 2C-SNOW-PROFILE. The number of matched CloudSat-ECCC observations in each bin is given in brackets.

increased mismatch at lower intensity precipitation. Except in a few cases caused by the spatio-temporal mismatch between CloudSat and ECCC weather data, it is unlikely for a human observer to miss heavy snowfall occurrences. This leads to an increase in accuracy at higher intensities.

2.4.3 Physical Factors Affecting POD

Next, we investigate the influence of reflectivity, temperature and altitude of the lowest cloud layer (cloud altitude) in deciding the accuracy as these variables form the basis of precipitation occurrence and phase detection in the CloudSat algorithm. Previous studies suggested the dependence of reflectivity and temperature thresholds in influencing the retrieval accuracy of CloudSat (Hudak et al., 2008; Hiley et al., 2010). Fig. 2.7 shows the distribution of near-surface reflectivity, near-surface temperature and the altitude of the lowest cloud layer to the surface retrieved by CloudSat, for the cases where ECCC

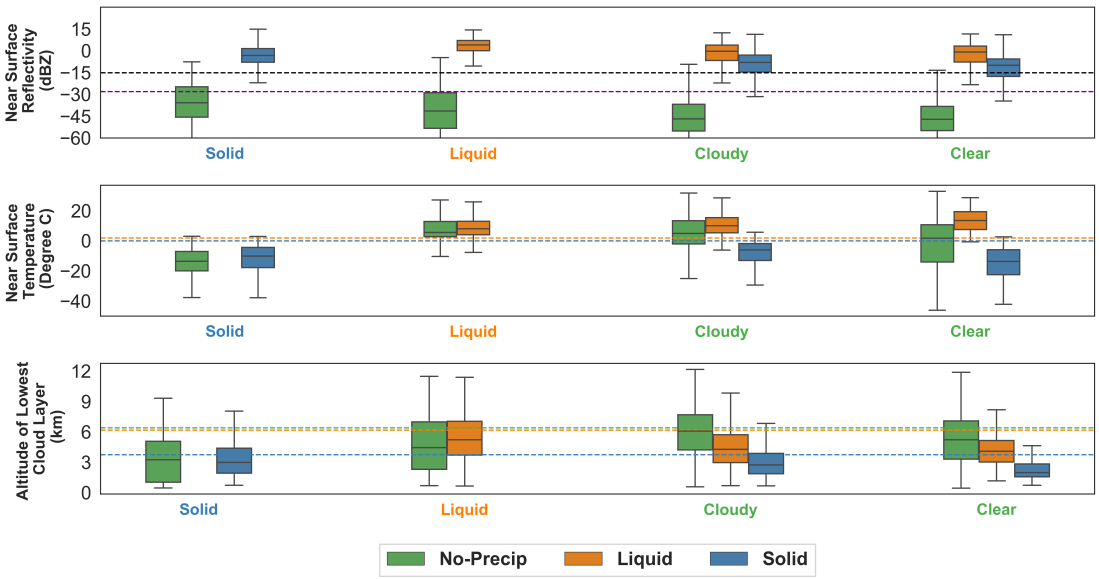

Figure 2.7: Box plots showing the distributions of CloudSat reflectivity, surface temperature and altitude of the lowest cloud layer for different ECCC weather types recorded on the ground across Canada. The dotted lines in (a) represent the minimum detectability limit of CloudSat-CPR (-28 dBZe) and the reflectivity threshold estimated by Haynes et al. (2009) for precipitation occurrence (-15 dBZe). The near-surface reflectivity <-60 dBZe (very low to produce precipitation) is not shown in the figure. The lines in (b) represent the temperature thresholds used in the CloudSat precipitation phase identification algorithm for classifying falling precipitation as snow (0 ^{o}C) and rain (2 ^{o}C) (Smalley et al., 2014). The lines in (c) show the mean altitude of cloud tops estimated for the cases where the CloudSat precipitation phases agreed with ECCC weather data. The no-precip category for solid and liquid include both the cases where CloudSat missed the precipitation occurrence and misclassified its phase, as explained in Section 2.4.3.

weather data recorded solid, liquid, cloudy and clear weather conditions. Solid and liquid types are obtained by combining the different types of solid and liquid precipitation types shown in Fig. 2.4 (b). Cloudy weather type is obtained by combining 'mainly cloudy' and 'cloudy' weather types in Fig. 2.4(b). Similarly, the clear weather type is obtained by combining 'clear' and 'mainly clear' weather conditions. Due to the low number of occurrences of CloudSat misclassifying ECCC observed solid precipitation as liquid (as

shown in Fig. 2.4(a) and (b)), the misclassified cases are excluded from this analysis. This gives us a binary classification where CloudSat accurately identified solid precipitation and CloudSat missed its occurrence. A similar procedure is followed to create a binary classification for the cases where CloudSat misclassified liquid precipitation occurrences as solid. However, due to a large number of occurrences where CloudSat misclassifying non-precipitating conditions (cloudy and clear) as either solid or liquid, the misclassified solid and liquid cases are represented by individual boxes in Fig. 2.7.

Table 2.5: Binomial and Multinomial logistic regression outputs showing coefficients and p values (given in parentheses) for solid, liquid, cloudy and clear weather conditions.

ECCC Weather	CloudSat Classification	Reflectivity	Temperature	Cloud Altitude	Regression Method
Solid	No-Precip	-0.1820 (<0.001)	0.0073 (0.0144)	-0.14778 (0.4976)	Binomial
Liquid	No-Precip	-0.1820 (<0.001)	-0.0230 (<0.001)	-0.2147 (<0.001)	Binomial
Clear	Solid	0.1114 (<0.001)	-0.0570 (0.1357)	-0.6131 (<0.001)	
	Liquid	0.1672 (<0.001)	0.1687 (0.0267)	-0.2753 (<0.001)	Multinomial
Cloudy					
	Solid	0.1252 (<0.001)	-0.1274 (<0.001)	-0.4374 (<0.001)	
	Liquid	0.1795 (<0.001)	0.1931 (<0.001)	-0.2319 (<0.001)	Multinomial

Fig. 2.7 shows that CloudSat retrieval agrees more closely with the ECCC weather type observations under precipitating clouds (Solid, Liquid) with relatively higher reflectivity and non-precipitating clouds (Cloudy, Clear) with lower reflectivity. To get a quantitative understanding of the influence of reflectivity, temperature and cloud altitude, binomial logistic regression testing is carried out for solid and liquid precipitation types and multinomial logistic regression for cloudy and clear weather conditions. The logistic regression coefficients and p-values are shown in Table 2.5. By using CloudSat classifying solid precipitation as a baseline, the binomial logistic regression outputs for solid precipitation show

that an increase in reflectivity and cloud altitude and a decrease in temperature increases the odds of CloudSat correctly classifying solid precipitation. The results make sense physically. Haynes et al. (2009) reported a reflectivity threshold of -15 dBZe for precipitation occurrence followed by an increase in the probability of observing precipitation with an increase in reflectivity above -15 dBZe. Therefore, the increase in reflectivity favours precipitation with its phase depends on temperature. The significance of reflectivity and temperature for solid precipitation are indicated by the low p-values as shown in Table 2.5.

Relative to CloudSat classifying liquid precipitation, the binomial logistic regression results for liquid precipitation show that an increase in reflectivity, temperature and cloud altitude increases the odds CloudSat correctly classifying liquid precipitation (Table 2.5). All the variables are significant here, as indicated by p values <0.05. The increase in cloud height increases the travel time of hydrometeors before reaching the ground surface. The increased travel time, coupled with an increase in temperature leads to the melting of hydrometeors to liquid (Dai, 2008). Keeping CloudSat classifying non-precipitating weather as the baseline, the multinomial logistic regression results for non-precipitating cloudy and clear weather conditions indicate that an increase in reflectivity and a decrease in cloud altitude and temperature, increases the odds of CloudSat misclassifying a non-precipitating cloud as solid precipitation. Similarly, an increase in reflectivity, and temperature and a decrease in cloud altitude increases the odds of CloudSat misclassifying a non-precipitating cloud as liquid precipitation.

2.5 Summary & Conclusions

This study describes the validation results of precipitation phase information retrieved by CloudSat using present weather data recorded on the ground by human observers (ECCC weather data) and POSS weather radar. The study validates phase estimates of CloudSat based on precipitation occurrence, weather types recorded on the ground, and prevailing precipitation intensity. Detailed studies are carried out at Eureka weather station due to the overlapping data availability from CloudSat, ECCC and POSS weather radar from 2006 to 2016. Later, the method is extended towards stations situated in lower latitudes to identify the pan-Canadian performance of CloudSat using ECCC weather data. Analysis is carried out to identify the influence of physical factors influencing validation accuracy using binomial and multinomial logistic regression.

CloudSat shows high accuracy in detecting precipitation phases, as indicated by high POD values across Canada. Mean POD values for solid, liquid and non-precipitating conditions at the 27 stations are 80.8%$\pm$1.5, 83.2%$\pm$1.9 and 69.8%$\pm$0.8 respectively. The study

shows that the POD varies with precipitation type, and is inversely proportional to cloud cover. The heaviest cloud cover produces the lowest POD. CloudSat tends to miss snow grains, drizzle and freezing drizzle more often than other types of precipitation. Next, we binned the collocated CloudSat-ECCC observations by the intensity of solid precipitation recorded by satellite and the results show that the accuracy of CloudSat increases with an increase in intensity. To understand the influence physical factors in influencing POD, we analyzed the distributions of near-surface reflectivity, temperature and altitude of lowest cloud layer retrieved by CloudSat for solid, liquid, cloudy and clear weather types recorded by ECCC. The results show that POD is higher for precipitating clouds with relatively high reflectivity and for non-precipitating clouds with lower reflectivity. Binomial and multinomial regression methods are employed to get quantitative information on the influence of physical factors. The regression outputs indicate that in addition to reflectivity and temperature, cloud top height also becomes significant in cases of liquid precipitation and non-precipitating conditions. Also, the results suggest a possible false positive detection by CloudSat related to reflectivity.

The reduction in POD values links back to the fundamental differences between CloudSat and ground-based datasets and the spatio-temporal mismatch introduced by the validation method. The high sensitivity of CloudSat enables it to detect very light precipitation intensities (<0.01 mm/hr), which sometimes fall as virga and remain undetected by ground-based observing systems. The phase identification methodology followed varies between datasets. CloudSat uses a complicated retrieval algorithm; POSS uses reflectivity based regression method and human observation in ECCC weather data. The sampling volume also varies, with POSS sampling limited to a maximum of 1 cubic metre above its sensor and human observations depend on the prevailing visibility. At the same time, CloudSat-CPR observes a narrow swath of cloud cover from an orbit placed 705km above the Earth's surface. These points need further exploration. But it is beyond the scope of this paper.

To the best of our knowledge, this study presents the first detailed phase validation approach of CloudSat using the ground-based human observed weather data across Canada. The precipitation-flag based phase identification methodology described in this paper is a reproducible method and is applicable at all locations with CloudSat coverage. The method comes useful in rain/snow partitioning studies and introduces a potential way to improve the phase representation in weather, climate or hydrologic models for locations with a limited amount of observational data. Moreover, CloudSat precipitation products, together with its auxiliary meteorological information, present itself as a large source of archived training data, which can be used to develop/ improve the phase partitioning algorithms using complex machine-learning based methods.

Chapter 3

Conclusions

We find high accuracy for CloudSat in classifying precipitation phases across Canada. The initial validation study at Eureka, NU using ECCC weather data shows POD values of 81.5%, 79% and 69% for solid, liquid and non-precipitating weather, respectively. An independent verification is performed at Eureka using the precipitation occurrence and phase estimation from the POSS sensor. When extended across Canada we find mean POD values of 80.8%±1.5, 83.2%±1.9 and 69.8%±0.8 for solid, liquid and non-precipitating weather respectively. The pan-Canada results are broadly consistent with those reported at Eureka. These results confirm that contamination by ground clutter in the boundary layer does not adversely affect the probability of detection (POD) from CloudSat.

To gain some in-depth information on the phase classification accuracy of CloudSat, we studied the influence of different precipitation/weather types on POD. The results show that the accuracy of CloudSat varies between different weather types observed on the ground with a notable decrease in accuracy under non-precipitating cloudy weather type. Also, the accuracy of CloudSat increases with an increase in solid precipitation intensity as indicated by the increase in POD from 34% (<0.01 mm/hr) to 85% (> 1mm/hr). By analyzing the distribution of near-surface reflectivity, we find higher accuracy for CloudSat in classifying precipitating clouds with reflectivity >-15dBZe and for non-precipitating clouds at relatively lower reflectivities. The multinomial and binomial regression outputs show statistically significant relationships for reflectivity associated with CloudSat's classification of solid, liquid and no-precipitation.

Chen et al. (2016) suggested a POD of ∼70% as reasonable when validating CloudSat precipitation phase estimates using other datasets of different spatial and temporal resolutions. Considering that, the results obtained in this study by validating CloudSat

using ground-based datasets at different temporal resolutions are quite promising. The results indicate that CloudSat can be used as a potential source of information for identifying the precipitation occurrence and its phase over the remote Arctic locations as well as pan-Canada. The high sensitivity of CloudSat allows it to capture the light snowfall events predominant in the Arctic, which is difficult for human observers to detect. The precipitation phase information from CloudSat can be used as a source for filling the gaps in observational data over these locations. Considering its high accuracy, the precipitation phase estimates from CloudSat can also be used as an independent source of validation for other present weather sensors and remote sensing satellites.

3.1 Future Work

The results from this study are influenced by the spatial radius used for collecting CloudSat overpasses and the spatial and temporal mismatch between CloudSat and ground-based datasets. The selected spatial radius should provide an optimum balance between sample size (number of overpasses) and distance from stations. In cases where it is necessary to have a larger spatial radius, defining a distance weighing function for giving more weight to retrievals close to the ground station with a decrease in weight as the satellite goes away from the station is desirable. This may help to reduce the spatial mismatch between CloudSat and ground-based datasets. Similarly, a temporal weighting approach to give more weight to the CloudSat retrievals closer in time to ground-based observations may improve the POD estimates from CloudSat. Similarly, other variables available from CloudSat, such as 'cloud mask', and 'data status', and how these can be used to remove the noise in the estimated POD need further exploration. However, these variables are scattered across different products of CloudSat, and some of these are available as a 2-Dimensional variable while some are 1-Dimensional. Therefore, suitable statistical methods need to be devised to make these variables and products comparable.

The high validation accuracy of the CloudSat dataset in the Arctic, as well as stations spread across Canada, present itself as a valuable source of information for studying the processes related to snow-rain phase transition across these latitudes. CloudSat precipitation flag information, along with the environmental variables (surface temperature, the vertical profile of temperature, pressure, humidity, etc.) available from ECMWF-AUX product from 2006 to the present day, can be used to train and develop machine learning models for predicting precipitation phase. After the initial validation and quality control, the developed models can be deployed in a modelling framework for estimating snowfall occurrence and subsequent estimation of snow properties such as Snow Water Equivalent

(SWE) and Snow Depth (SD). The representation of precipitation phase in land surface and hydrological models are critical. Previous studies have identified biases in the model outputs of SWE and SD related to precipitation phase representation (Behrangi et al., 2018; Wen et al., 2013; Currier et al., 2017; Wrzesien et al., 2017). Reducing the uncertainties related to model outputs will help to provide a better insight into how the snow properties are evolving under the changing climate. The machine learning models for predicting precipitation phases developed using CloudSat will be useful to address some of these uncertainties and to get a clearer picture of changing snow cover in the Arctic.

References

Barnett, T. P., Adam, J. C., and Lettenmaier, D. P. (2005). Potential impacts of a warming climate on water availability in snow-dominated regions. *Nature*, 438(7066):303–309.

Behrangi, A., Lebsock, M., Wong, S., and Lambrigtsen, B. (2012). On the quantification of oceanic rainfall using spaceborne sensors. *Journal of Geophysical Research: Atmospheres*, 117(D20).

Behrangi, A., Tian, Y., Lambrigtsen, B. H., and Stephens, G. L. (2014). What does CloudSat reveal about global land precipitation detection by other spaceborne sensors? *Water Resources Research*, 50(6):4893–4905.

Behrangi, A., Yin, X., Rajagopal, S., Stampoulis, D., and Ye, H. (2018). On distinguishing snowfall from rainfall using near-surface atmospheric information: Comparative analysis, uncertainties and hydrologic importance. *Quarterly Journal of the Royal Meteorological Society*, 144(S1):89–102.

Bintanja, R. (2018). The impact of Arctic warming on increased rainfall. *Scientific Reports*, 8.

Birkeland, K. W. and Mock, C. J. (1996). Atmospheric Circulation Patterns Associated with Heavy Snowfall Events, Bridger Bowl, Montana, U.S.A. *Mountain Research and Development*, 16(3):281–286.

Cao, Q., Hong, Y., Chen, S., Gourley, J. J., Zhang, J., and Kirstetter, P. E. (2014). Snowfall Detectability Of Nasa's Cloudsat: The First Cross-Investigation Of Its 2c-Snow-Profile Product And National Multi-Sensor Mosaic Qpe (Nmq) Snowfall Data. *Progress In Electromagnetics Research*, 148:55–61.

Castellani, B. B., Shupe, M. D., Hudak, D. R., and Sheppard, B. E. (2015). The annual cycle of snowfall at Summit, Greenland. *Journal of Geophysical Research: Atmospheres*, 120(13):6654–6668.

Chen, A., Leptoukh, G., Di, L., Nadeau, D., Farley, J., Lynnes, C., and Kempler, S. (2007). Visualization of and Access to CloudSat Vertical Data through Google Earth. *Nature Precedings*, pages 1–1.

Chen, S., Hong, Y., Kulie, M., Behrangi, A., Stepanian, P. M., Cao, Q., You, Y., Zhang, J., Hu, J., and Zhang, X. (2016). Comparison of snowfall estimates from the NASA CloudSat Cloud Profiling Radar and NOAA/NSSL Multi-Radar Multi-Sensor System. *Journal of Hydrology*, 541:862–872.

Clothiaux, E. E. and Miller, M. A. (1994). An Evaluation of a 94-GHz Radar for Remote Sensing of Cloud Properties: Journal of Atmospheric and Oceanic Technology: Vol 12, No 2. *Journal of Atmospheric and Oceanic Technology*.

Cronk, H. and Partain, P. (2017). CloudSat ECMWF-AUX Auxillary Data ProductProcess Description and Interface Control Document. Technical report, Colorado State University.

Currier, W. R., Thorson, T., and Lundquist, J. D. (2017). Independent Evaluation of Frozen Precipitation from WRF and PRISM in the Olympic Mountains. *Journal of Hydrometeorology*, 18(10):2681–2703.

Dai, A. (2008). Temperature and pressure dependence of the rain-snow phase transition over land and ocean. *Geophysical Research Letters*, 35(12):L12802.

Derksen, C., Smith, S. L., Sharp, M., Brown, L., Howell, S., Copland, L., Mueller, D. R., Gauthier, Y., Fletcher, C. G., Tivy, A., Bernier, M., Bourgeois, J., Brown, R., Burn, C. R., Duguay, C., Kushner, P., Langlois, A., Lewkowicz, A. G., Royer, A., and Walker, A. (2012). Variability and change in the Canadian cryosphere. *Climatic Change*, 115(1):59–88.

Derksen, C. and Walker, A. E. (2003). Identification of systematic bias in the cross-platform (SMMR and SSM/I) EASE-Grid brightness temperature time series. *IEEE Transactions on Geoscience and Remote Sensing*, 41(4):910–915.

Dietz, A. J., Kuenzer, C., Gessner, U., and Dech, S. (2012). Remote sensing of snow – a review of available methods. *International Journal of Remote Sensing*, 33(13):4094–4134.

ECCC (2011). Glossary - Climate - Environment and Climate Change Canada.

ECMWF (2019). IFS Documentation CY46r1. In *ECMWF Forecast User Guide*. ECMWF.

Fall, V. M., Cao, Q., and Hong, Y. (2013). Intercomparison of Vertical Structure of Storms Revealed by Ground-Based (NMQ) and Spaceborne Radars (CloudSat-CPR and TRMM-PR). *The Scientific World Journal*, 2013.

Fargey, S., Henson, W., Hanesiak, J., and Goodson, R. (2014). Characterization of an unexpected snowfall event in Iqaluit, Nunavut, and surrounding area during the Storm Studies in the Arctic field project.

Field, P. R. and Heymsfield, A. J. (2015). Importance of snow to global precipitation. *Geophysical Research Letters*, 42(21):9512–9520.

Flanner, M. G., Shell, K. M., Barlage, M., Perovich, D. K., and Tschudi, M. A. (2011). Radiative forcing and albedo feedback from the Northern Hemisphere cryosphere between 1979 and 2008. *Nature Geoscience*, 4(3):151–155.

Foster, J. L., Sun, C., Walker, J. P., Kelly, R., Chang, A., Dong, J., and Powell, H. (2005). Quantifying the uncertainty in passive microwave snow water equivalent observations. *Remote Sensing of Environment*, 94(2):187–203.

Haynes, J. M., L'Ecuyer, T. S., Stephens, G. L., Miller, S. D., Mitrescu, C., Wood, N. B., and Tanelli, S. (2009). Rainfall retrieval over the ocean with spaceborne W-band radar. *Journal of Geophysical Research: Atmospheres*, 114(D8).

Haynes, J. M. and L'Ecuyer, T. (2013). Level 2-C Precipitation Column Algorithm Product Process Description and Interface Control Document.

Hiley, M. J., Kulie, M. S., and Bennartz, R. (2010). Uncertainty Analysis for CloudSat Snowfall Retrievals. *Journal of Applied Meteorology and Climatology*, 50(2):399–418.

Hiley, M. J., Kulie, M. S., and Bennartz, R. (2011). Uncertainty Analysis for *CloudSat* Snowfall Retrievals. *Journal of Applied Meteorology and Climatology*, 50(2):399–418.

Hudak, D., Rodriguez, P., and Donaldson, N. (2008). Validation of the CloudSat precipitation occurrence algorithm using the Canadian C band radar network. *Journal of Geophysical Research: Atmospheres*, 113(D8):D00A07.

Intrieri, J. M. and Shupe, M. D. (2004). Characteristics and Radiative Effects of Diamond Dust over the Western Arctic Ocean Region. *Journal of Climate*, 17(15):2953–2960.

Jennings, K. S., Winchell, T. S., Livneh, B., and Molotch, N. P. (2018). Spatial variation of the rain–snow temperature threshold across the Northern Hemisphere. *Nature Communications*, 9(1).

Kongoli, C., Romanov, P., and Ferraro, R. (2012). Snow Cover Monitoring from Remote-Sensing Satellites: Possibilities for Drought Assessment. In *Remote Sensing of Drought: Innovative Monitoring Approaches*, pages 359–383. Publications, Agencies and Staff of the U.S. Department of Commerce.

Kulie, M. S. and Bennartz, R. (2009). Utilizing Spaceborne Radars to Retrieve Dry Snowfall. *Journal of Applied Meteorology and Climatology*, 48(12):2564–2580.

Kulie, M. S., Milani, L., Wood, N. B., Tushaus, S. A., Bennartz, R., and L'Ecuyer, T. S. (2016). A Shallow Cumuliform Snowfall Census Using Spaceborne Radar. *Journal of Hydrometeorology*, 17(4):1261–1279.

Kushner, P. J., Mudryk, L. R., Merryfield, W., Ambadan, J. T., Berg, A., Bichet, A., Brown, R., Derksen, C., Déry, S. J., Dirkson, A., Flato, G., Fletcher, C. G., Fyfe, J. C., Gillett, N., Haas, C., Howell, S., Laliberté, F., McCusker, K., Sigmond, M., Sospedra-Alfonso, R., Tandon, N. F., Thackeray, C., Tremblay, B., and Zwiers, F. W. (2018). Canadian snow and sea ice: assessment of snow, sea ice, and related climate processes in Canada's Earth system model and climate-prediction system. *The Cryosphere*, 12(4):1137–1156.

König, M., Winther, J.-G., and Isaksson, E. (2001). Measuring snow and glacier ice properties from satellite. *Reviews of Geophysics*, 39(1):1–27.

Lesbock, M. (2018). Level 2c RAIN-PROFILE Product Process Description and Interface Control Document. Technical report, NASA.

Lesins, G., Duck, T. J., and Drummond, J. R. (2010). Climate trends at Eureka in the Canadian high arctic. *Atmosphere-Ocean*, 48(2):59–80.

Liu, G. (2008). Deriving snow cloud characteristics from CloudSat observations. *Journal of Geophysical Research: Atmospheres*, 113(D8).

Liu, Y., Li, L., Yang, J., Chen, X., and Hao, J. (2017). Estimating Snow Depth Using Multi-Source Data Fusion Based on the D-InSAR Method and 3dvar Fusion Algorithm. *Remote Sensing*, 9(11):1195.

Marchand, R., Mace, G. G., Ackerman, T., and Stephens, G. (2008). Hydrometeor Detection Using *Cloudsat* —An Earth-Orbiting 94-GHz Cloud Radar. *Journal of Atmospheric and Oceanic Technology*, 25(4):519–533.

Matrosov, S. Y. (2014). Intercomparisons of *CloudSat* and Ground-Based Radar Retrievals of Rain Rate over Land. *Journal of Applied Meteorology and Climatology*, 53(10):2360–2370.

Matrosov, S. Y. and Battaglia, A. (2009). Influence of multiple scattering on CloudSat measurements in snow: A model study. *Geophysical Research Letters*, 36(12):L12806.

Mekis, E., Donaldson, N., Reid, J., Zucconi, A., Hoover, J., Li, Q., Nitu, R., and Melo, S. (2018). An Overview of Surface-Based Precipitation Observations at Environment and Climate Change Canada. *Atmosphere-Ocean*, 56(2):71–95.

Merenti-Välimäki, H.-L., Lönnqvist, J., and Laininen, P. (2001). Present weather: comparing human observations and one type of automated sensor. *Meteorological Applications*, 8(4):491–496.

Meteorological Service of Canada (2015). *MANOBS - manual of surface weather observations.* OCLC: 907906587.

Mizukami, N., Koren, V., Smith, M., Kingsmill, D., Zhang, Z., Cosgrove, B., and Cui, Z. (2013). The Impact of Precipitation Type Discrimination on Hydrologic Simulation: Rain–Snow Partitioning Derived from HMT-West Radar-Detected Brightband Height versus Surface Temperature Data. *Journal of Hydrometeorology*, 14(4):1139–1158.

Mudryk, L. R., Derksen, C., Howell, S., Laliberté, F., Thackeray, C., Sospedra-Alfonso, R., Vionnet, V., Kushner, P. J., and Brown, R. (2018). Canadian snow and sea ice: historical trends and projections. *The Cryosphere*, 12(4):1157–1176.

Norin, L., Devasthale, A., L'Ecuyer, T. S., Wood, N. B., and Smalley, M. (2015). Intercomparison of snowfall estimates derived from the CloudSat Cloud Profiling Radar and the ground-based weather radar network over Sweden. *Atmospheric Measurement Techniques*, 8(12):5009–5021.

Palerme, C., Claud, C., Dufour, A., Genthon, C., Wood, N. B., and L'Ecuyer, T. (2017). Evaluation of Antarctic snowfall in global meteorological reanalyses. *Atmospheric Research*, 190:104–112.

Robinson, D. and Frei, A. (2000). Seasonal Variability of Northern Hemisphere Snow Extent Using Visible Satellite Data. *The Professional Geographer*, 52(2):307–315.

Rosato, D. and Rosato, D. (2003). *Plastics Engineered Product Design.* Elsevier.

Sassen, K., Matrosov, S., and Campbell, J. (2007). CloudSat spaceborne 94 GHz radar bright bands in the melting layer: An attenuation-driven upside-down lidar analog. *Geophysical Research Letters*, 34(16).

Sheppard, B. E. (2007). Sampling Errors in the Measurement of Rainfall Parameters Using the Precipitation Occurrence Sensor System (POSS). *Journal of Atmospheric and Oceanic Technology*, 24(2):125–140.

Sheppard, B. E. and Joe, P. I. (1994). Comparison of Raindrop Size Distribution Measurements by a Joss-Waldvogel Disdrometer, a PMS 2dg Spectrometer, and a POSS Doppler Radar. *Journal of Atmospheric and Oceanic Technology*, 11(4):874–887.

Sheppard, B. E. and Joe, P. I. (2000). Automated Precipitation Detection and Typing in Winter: A Two-Year Study. *Journal of Atmospheric and Oceanic Technology*, 17(11):1493–1507.

Sheppard, B. E. and Joe, P. I. (2008). Performance of the Precipitation Occurrence Sensor System as a Precipitation Gauge. *Journal of Atmospheric and Oceanic Technology*, 25(2):196–212.

Shi, J. (2008). Active Microwave Remote Sensing Systems and Applications to Snow Monitoring. In Liang, S., editor, *Advances in Land Remote Sensing: System, Modeling, Inversion and Application*, pages 19–49. Springer Netherlands, Dordrecht.

Slonosky, V. (2014). Historical climate observations in Canada: 18th and 19th century daily temperature from the St. Lawrence Valley, Quebec. *Geoscience Data Journal*, 1(2):103–120.

Smalley, M., L'Ecuyer, T., Lebsock, M., and Haynes, J. (2013). A Comparison of Precipitation Occurrence from the NCEP Stage IV QPE Product and the CloudSat Cloud Profiling Radar. *Journal of Hydrometeorology*, 15(1):444–458.

Smalley, M., L'Ecuyer, T., Lebsock, M., and Haynes, J. (2014). A Comparison of Precipitation Occurrence from the NCEP Stage IV QPE Product and the *CloudSat* Cloud Profiling Radar. *Journal of Hydrometeorology*, 15(1):444–458.

Stephens, G. and Wood, N. (2013). Level 2c Snow Profile Process Description and Interface Control Document. *NASA*, page 21.

Stephens, G. L., Li, J., Wild, M., Clayson, C. A., Loeb, N., Kato, S., L'Ecuyer, T., Stackhouse, P. W., Lebsock, M., and Andrews, T. (2012). An update on Earth's energy balance in light of the latest global observations. *Nature Geoscience*, 5(10):691–696.

Stephens, G. L., Vane, D. G., Boain, R. J., Mace, G. G., Sassen, K., Wang, Z., Illingworth, A. J., O'connor, E. J., Rossow, W. B., Durden, S. L., Miller, S. D., Austin, R. T., Benedetti, A., and Mitrescu, C. (2002). The cloudsat mission and the a-train. *Bulletin of the American Meteorological Society*, 83(12):1771–1790.

Stephens, G. L., Vane, D. G., Tanelli, S., Im, E., Durden, S., Rokey, M., Reinke, D., Partain, P., Mace, G. G., Austin, R., L'Ecuyer, T., Haynes, J., Lebsock, M., Suzuki, K., Waliser, D., Wu, D., Kay, J., Gettelman, A., Wang, Z., and Marchand, R. (2008). CloudSat mission: Performance and early science after the first year of operation. *Journal of Geophysical Research: Atmospheres*, 113(D8):D00A18.

Tang, L., Tian, Y., and Lin, X. (2014). Validation of precipitation retrievals over land from satellite-based passive microwave sensors. *Journal of Geophysical Research: Atmospheres*, 119(8):4546–4567.

Thackeray, C. W., Fletcher, C. G., and Derksen, C. (2014). The influence of canopy snow parameterizations on snow albedo feedback in boreal forest regions: Boreal forest snow albedo feedback. *Journal of Geophysical Research: Atmospheres*, 119(16):9810–9821.

Thackeray, C. W., Fletcher, C. G., and Derksen, C. (2015). Quantifying the skill of CMIP5 models in simulating seasonal albedo and snow cover evolution: CMIP5-SIMULATED ALBEDO AND SCF SKILL. *Journal of Geophysical Research: Atmospheres*, 120(12):5831–5849.

Wang, X. L., Xu, H., Qian, B., Feng, Y., and Mekis, E. (2017). Adjusted Daily Rainfall and Snowfall Data for Canada. *Atmosphere-Ocean*, 55(3):155–168.

Wang, Y., You, Y., and Kulie, M. (2018). Global Virga Precipitation Distribution Derived From Three Spaceborne Radars and Its Contribution to the False Radiometer Precipitation Detection. *Geophysical Research Letters*, 45(9):4446–4455.

Wayand, N. E., Clark, M. P., and Lundquist, J. D. (2017). Diagnosing snow accumulation errors in a rain-snow transitional environment with snow board observations. *Hydrological Processes*, 31(2):349–363.

Wen, L., Nagabhatla, N., Lü, S., and Wang, S.-Y. (2013). Impact of rain snow threshold temperature on snow depth simulation in land surface and regional atmospheric models. *Advances in Atmospheric Sciences*, 30(5):1449–1460.

Wen, Y., Behrangi, A., Lambrigtsen, B., and Kirstetter, P.-E. (2016). Evaluation and Uncertainty Estimation of the Latest Radar and Satellite Snowfall Products Using SNOTEL

Measurements over Mountainous Regions in Western United States. *Remote Sensing*, 8(11):904.

Wood, N. B. (2011). *Estimation of Snow Microphysical Properties with Application to Millimeter-Wavelength Radar Retrievals for Snowfall Rate*. PhD thesis.

Wood, N. B., L'Ecuyer, T. S., Heymsfield, A. J., Stephens, G. L., Hudak, D. R., and Rodriguez, P. (2014). Estimating snow microphysical properties using collocated multisensor observations. *Journal of Geophysical Research: Atmospheres*, 119(14):8941–8961.

Wrzesien, M. L., Durand, M. T., Pavelsky, T. M., Howat, I. M., Margulis, S. A., and Huning, L. S. (2017). Comparison of Methods to Estimate Snow Water Equivalent at the Mountain Range Scale: A Case Study of the California Sierra Nevada. *Journal of Hydrometeorology*, 18(4):1101–1119.

You, Y., Wang, N.-Y., Ferraro, R., and Rudlosky, S. (2017). Quantifying the Snowfall Detection Performance of the GPM Microwave Imager Channels over Land. *Journal of Hydrometeorology*, 18(3):729–751.

Young, K. L., Brown, L., and Labine, C. (2018). Snow cover variability at Polar Bear Pass, Nunavut. *Arctic Science*, 4(4):669–690.

Zhu, L., Suomalainen, J., Liu, J., Hyyppä, J., Kaartinen, H., and Haggren, H. (2017). A Review: Remote Sensing Sensors. *Multi-purposeful Application of Geospatial Data*.